J Solid State Electrochem (1997) 1: 161 – 171

ORIGINAL PAPER

M. Bojinov

Modelling the formation and growth of anodic passive films on metals in concentrated acid solutions

Received: 24 January 1997 / Accepted: 18 April 1997

Abstract Two model approaches to the formation of passive films as adsorbed layers during the active anodic dissolution of a metal in acid and their subsequent growth are presented. The first depicts passivation as proceeding in parallel to active dissolution. Adsorption of water on active surface sites leads to passivation, whereas adsorption of acid leads to active dissolution of the metal. The model is consistent with the impedance response during passivation of Fe and an Fe-20%Mo alloy in concentrated H_3PO_4. The second model is an updated version of the so-called surface charge approach to the mechanism of conduction of anodic passive films. It is based on the assumptions that oxygen vacancies are the main ionic charge carriers and the field strength in the barrier layer is constant. A negative surface charge built up at the film/solution interface via accumulation of metal vacancies accelerates oxygen vacancy transport, thus explaining the pseudoinductive behaviour of the metal/film/electrolyte system under small amplitude a.c. perturbation. The model describes the growth of thin anodic films on Fe, Mo and an Fe-20%Mo alloy in concentrated H_3PO_4.

Key words Passivation · Anodic film· Surface charge · A.C. impedance · Kinetic model

Introduction

Passivation/activation dynamics at the metal/solution interface during anodic film formation and growth induces phenomena of fundamental interest, such as current oscillations and chemical breakdown via adsorption/incorporation of anions from the solution. On the other hand, anodic layer formation/dissolution processes on technical metals and alloys acquire major practical significance due to their application in electropolishing and associated technologies [1].

There were several attempts to use impedance measurements in the characterisation of passivation of metals in concentrated solutions [2–6]. A peculiar feature of the obtained impedance spectra circling the origin of the complex plane was observed for a range of metals in such solutions [2–5]. This feature was first detected by Epelboin [2] during transpassive dissolution and electropolishing of Ni in a range of H_2SO_4 solutions. A qualitative approach to the transpassivity of Ni was proposed by Epelboin and Keddam [7], introducing competitive passivation/dissolution reactions at the anodic film/electrolyte interface as electrically equivalent to a second-order dynamic behaviour of the electrochemical system. Several years ago, a revised kinetic model for the transpassivity of Ni was advanced by Keddam et al. [8] explaining the second-order dynamic behaviour in this special case only. Our research group registered similar impedance diagrams circling the complex plane origin during primary passivity of antimony [9], as well as the active/passive transition and the passive state of tin [10, 11] in concentrated H_2SO_4 solutions. A recent generalized model of the anodic oxidation of metals in concentrated solutions was able to explain this peculiar impedance locus [12]. It emphasized the coupled growth/dissolution processes of a continuous film at its interface with the electrolyte, leading to a second-order dynamic behaviour of the metal/film/solution system. Model predictions were consistent with a large set of impedance data for the passive state of Cu and Sb in concentrated H_2SO_4 [12]. The circling behaviour during the active-to-passive transition, however, remained unexplained within the frames of the proposed approach [10, 12]. To assess this special case, the possibility of simultaneous dissolution and passivation processes occurring on an initially bare metal surface should be taken into account.

M. Bojinov (✉)
Central Laboratory of Electrochemical Power Sources,
Bulgarian Academy of Science, Acad. G. Bonchev Str. bl.10,
1113 Sofia, Bulgaria

At higher overpotentials, a continuous barrier-like layer is formed on the metal surface, and transport processes in its bulk become predominant in the response of the electrode system. To describe the conduction mechanism in the passive state, we presented the so-called surface charge approach to the growth and relaxation in anodic films on metals [13–15]. This model succeeded in describing the anodic oxidation of Bi in glycol-borate electrolyte and Sn in concentrated sulphuric acid [15]. An extension of the model taking into account the kinetic role of the positive surface charge at the barrier layer/electrolyte interface was found to be consistent with the impedance response of passive Bi and Sb in the same medium [16].

In this connection, the following general purposes of the present work can be outlined:

1. To propose kinetic models of the anodic oxidation of metals in concentrated solutions in the passivation and the passivity range, respectively, and corresponding procedures for the determination of their parameters from experimental data
2. To collect voltammetric and impedance data for Fe, Mo and an Fe-Mo alloy in concentrated H_3PO_4 solutions in the potential ranges of interest and to compare them with the model predictions, thus testing the abilities of the models to describe the anodic behaviour of metals and alloys.

Theory

Passivation of metals in concentrated acid solutions

The quantitative model presented below is a modification of that advanced for the simultaneous growth/dissolution of a thin passive film in concentrated acid solutions [12] and is somewhat analogous to the model of passivation of Cr in H_2SO_4 proposed by Dobelaar and De Wit [17–20]. It is illustrated by a skeletal scheme in Fig. 1a.

The formation of the dissolution intermediate $Me(I)_{ad}$ is assumed to proceed via adsorption of an acid anion on an active surface site, and its oxidative desorption/dissociation generates soluble Me(II). Alternatively, an intermediate of the passivation reaction is formed when a water molecule is adsorbed on the active surface site. This reaction is assumed to be reversible but not necessarily in pseudo-equilibrium. The K_4 reaction represents the self-catalytic dissolution of metal ions through the fraction of the surface covered by the passivating species

$$Me + Me(II)_{pass} \rightarrow Me(II)_{sol} + Me(II)_{pass} + 2e^-$$

The assumption of Langmuir adsorption of intermediate species and Tafel dependence of the reaction rate constants on the overpotential E (expressed versus the rest potential which is thought to coincide with the equilibrium potential of step 1): $K_i = K_i^o \exp(\pm b_i E)$, $i = 1, 2, 3, 4, -1, -3$, where K_i^o are standard rate constants and b_i the Tafel coefficients, leads to the following balances at the inter-face.

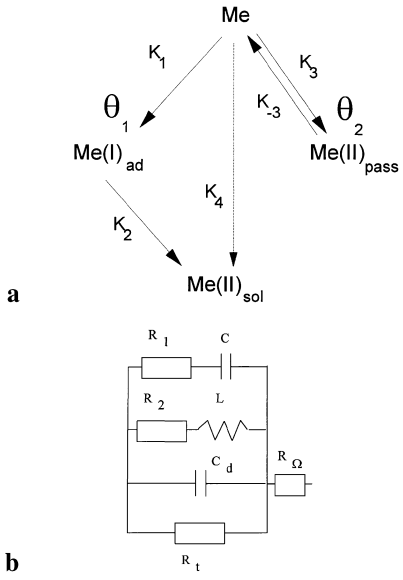

Fig. 1 A kinetic scheme of the proposed model for the passivation of metals and alloys in concentrated acid solutions (**a**) and the corresponding equivalent electrical circuit of the impedance response of the metal/solution interface (**b**)

$$i = F[K_1(1-\theta_1-\theta_2) + K_2\theta_1] + 2F[K_3(1-\theta_2) - K_{-3}\theta_2 + K_4\theta_2] \quad (1)$$

$$\beta\, d\theta_1/dt = K_1(1-\theta_1-\theta_2) - K_2\theta_1 \quad (2)$$

$$\beta\, d\theta_2/dt = K_3(1-\theta_2) - K_{-3}\theta_2 \quad (3)$$

where β is the maximum surface excess of adsorbed species.

The steady-state solution is obtained by setting the above time derivatives to zero:

$$i_s = 2F(K_2\theta_{1s} + K_4\theta_{2s}) \quad (4)$$

$$\theta_{1s} = K_1K_{-3}/(K_1+K_2)(K_3+K_{-3}) \quad (5)$$

$$\theta_{2s} = K_3/(K_3+K_{-3}) \quad (6)$$

The faradaic impedance is derived from the Taylor expansion of Eqs. 1–3 to the first order

$$Z_F^{-1} = R_t^{-1} + F[(K_2-K_1)\, d\theta_1/dE + 2(K_4-K_{-3}-K_3)\, d\theta_2/dE] \quad (7)$$

$$d\theta_1/dE = [K_1b_1(1-\theta_{1s}-\theta_{2s}) - K_2b_2\theta_{1s} - b_1K_1 d\theta_2/dE] \,/\, (j\omega\beta + K_1 + K_2)$$

$$d\theta_2/dE = [K_3b_3(1-\theta_{2s}) - K_{-3}b_{-3}\theta_{2s}]/(j\omega\beta + K_3 + K_{-3})$$

In order to obtain the total interfacial impedance, the double layer capacitance C_d and the electrolyte resistance R_Ω have to be appropriately added to the faradaic impedance

$$Z = (Z_F^{-1} + j\omega C_d)^{-1} + R_\Omega \tag{8}$$

The impedance expression is mathematically equivalent to the electrical circuit presented in Fig. 1b. The relations between circuit elements and kinetic constants are as follows

$$\begin{aligned} R_t^{-1} + R_1^{-1} &= F(b_1 + b_2)K_2\theta_{1s} \\ &\quad + 2F[(b_3 - b_{-3})K_{-3} + K_4 b_4]\theta_{2s} \\ C &= -\beta F[2(K_4 - K_{-3} - K_3) - K_1] \\ &\quad (b_3 - b_{-3})K_{-3}\theta_{2s}/(K_3 + K_{-3})^2 \\ R_2^{-1} &= F(K_2 - K_1)[(b_1 - b_2)K_2\theta_{1s}(K_3 + K_{-3}) \\ &\quad - K_1(b_3 - b_{-3})K_{-3}\theta_{2s}]/(K_3 + K_{-3})(K_1 + K_2) \\ L^{-1} &= F(K_2 - K_1)[(b_1 - b_2)K_2\theta_{1s}(K_3 + K_{-3}) \\ &\quad - K_1(b_3 - b_{-3})K_{-3}\theta_{2s}]/(K_3 + K_{-3})\beta \end{aligned} \tag{9}$$

A numerical procedure for the determination of the kinetic constants was developed. As a first step the elements of the equivalent circuit (Fig. 1b) are calculated for a range of potentials using a software package for equivalent circuit analysis elaborated by the author. Using the potential dependence of the circuit elements, the system of equations Eqs. 4–6 and 9, is resolved by a non-linear least-squares fitting procedure providing values for the kinetic constants. The ability of this procedure will be tested against the experimental data for the passivation process of Fe and a Fe-20%Mo alloy in concentrated phosphoric acid.

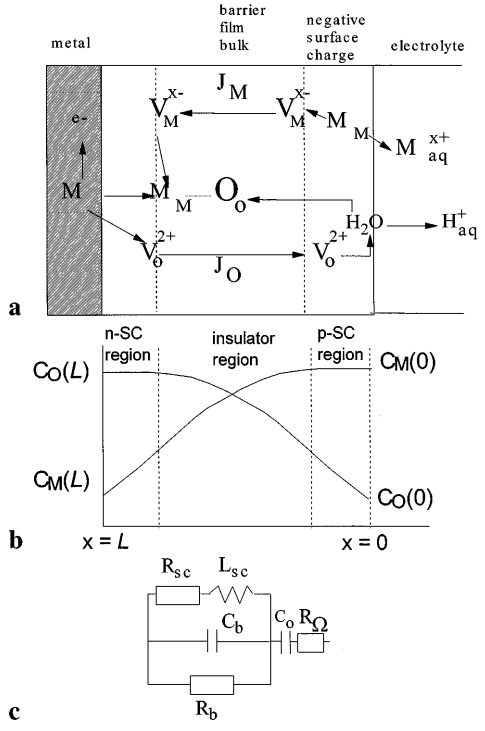

Fig. 2 Scheme of the processes in the metal/anodic film/electrolyte system according to the surface charge approach (**a**), proposed distribution of the concentrations of the oxygen and metal vacancies in the anodic film (**b**) and equivalent circuit of the impedance response predicted by the surface charge approach (**c**). For the physical meaning of the symbols see text

Passive state of metals – the surface charge approach

A scheme of the main processes in the metal/anodic oxide/solution system according to the surface charge approach is presented in Fig. 2a.

At the metal/film interface, oxidation of the metal to a metal position in the oxide network with injection of oxygen vacancies takes place [19–23] (the Kroeger-Vink notation is used). Oxygen vacancies are transported through the film and react with adsorbed water at the film/solution interface [19–23]. Accordingly, metal vacancies are produced at the film/solution interface via abstraction of a metal position from the oxide network and are consumed at the metal/film boundary, restoring the metal position.

We accepted the ideas of Macdonald et al. [19, 21–23] in what concerns the chemistry of the interfacial reactions and two of the basic assumptions: (a) that the mean electric field $\boldsymbol{E}$ is independent of the applied potential and film thickness, and (b) that the film grows via transport of oxygen vacancies. Instead of using the Nernst-Planck transport equations proposed in [19, 23] we will treat the vacancy motion mechanism in a more general way as described by Fromhold [24].

In a coordinate system with $x = 0$ at the film/solution interface and $x = L$ at the metal/film interface [19], where L is the film thickness (Fig. 2a, b), the flux of oxygen vacancies is given by the differential equation [24]

$$\begin{aligned} J_O(x) &= -D_O(\mathrm{d}c_O(x)/\mathrm{d}x)\mathrm{ch}[zFa\boldsymbol{E}(x)/RT] \\ &\quad - (D_O/a)c_O(x)\mathrm{sh}[zFa\boldsymbol{E}(x)/RT] \end{aligned} \tag{10}$$

where D_O is the diffusivity of oxygen vacancies

$$D_O = 4a^2 f \exp(-A/RT) \tag{11}$$

c_O is their concentration, a is the half-jump distance, A is the zero field activation energy for vacancy motion, f is the hopping frequency, and the other symbols have their usual meanings.

Solving this equation with the appropriate boundary conditions in a homogeneous field approximation ($\boldsymbol{E}(x) = \mathrm{const}$) gives [24]

$$\begin{aligned} J_O &= (D_O/a)\mathrm{sh}(zFa\boldsymbol{E}_L/RT)\{c_O(0) \\ &\quad \exp[-(L/a)\mathrm{th}(zFa\boldsymbol{E}_L/RT)] \\ &\quad - c_O(L)\}/\{1 - \exp[-(L/a)\mathrm{th}(zFa\boldsymbol{E}_L/RT)]\} \end{aligned} \tag{12}$$

where $\boldsymbol{E}_L$ is the field at the metal/film interface, $c_O(0)$ is the concentration of oxygen vacancies at the film/solution interface and $c_O(L)$ is their concentration at the metal/film interface. Solving for $c_O(L)$ results in the expression

$$c_O(L) = c_O(0)\exp[-(L/a)\mathrm{th}(zFa\boldsymbol{E}_L/RT)] - [a/D_O\mathrm{sh}(zFa\boldsymbol{E}_L/RT)] J_O\{1-\exp[-(L/a)\mathrm{th}(zFa\boldsymbol{E}_L/RT)]\} \quad (13)$$

An analogous expression can be written for the concentration of metal vacancies. This furnishes the possibility of representing the anodic film as consisting of three parts: a region of almost constant oxygen vacancy concentration at the metal/film interface (n-semiconductor part), an insulating part of the layer where both positive and negative defect concentrations decay exponentially, and a corresponding region of almost constant metal vacancy concentration at the film/solution interface (p-semiconductor part) (Fig. 2b) [19]. Since oxygen vacancy transport is assumed to be much faster than that of metal vacancies, the accumulation of the latter at the film/electrolyte boundary to form a negative surface charge q_n is physically justified [16].

At this stage, two limiting cases are usually considered [24]:

1. High-field limit: $zFa\boldsymbol{E}_L/RT \gg 1, \mathrm{th}(zFa\boldsymbol{E}_L/RT) = 1$ and $\mathrm{sh}(zFa\boldsymbol{E}_L/RT) = \exp(zFa\boldsymbol{E}_L/RT)/2$. Eq. 13 is transformed to yield

$$c_O(L) = c_O(0)\exp[-(L/a)] - [2a/D_O\exp(zFa\boldsymbol{E}_L/RT)] J_O\{1-\exp[-(L/a)]\} \quad (14)$$

Furthermore, as for all cases $L \gg a$, we finally get

$$c_O(L) = c_O(0)\exp[-(L/a)] - 2aJ_O/D_O\exp(zFa\boldsymbol{E}_L/RT) \quad (15)$$

2. Low-field limit: $zFa\boldsymbol{E}_L/RT \ll 1$, $\mathrm{th}(zFa\boldsymbol{E}_L/RT) = zFa\boldsymbol{E}_L/RT$ and $\mathrm{sh}(zFa\boldsymbol{E}_L/RT) = zFa\boldsymbol{E}_L/RT$. In this limit, it follows from Eq. 13 that

$$c_O(L) = c_O(0)\exp[-(zF\boldsymbol{E}_L L/RT)] - RTJ_O/D_O zF\boldsymbol{E}_L \quad (16)$$

which is exactly the result obtained by Macdonald et al. [23]. Following their ideas, we assume that $c_O(L) = N_D(E)$, where N_D is the density of donors in the n-semiconductor region adjacent to the metal/film interface [23]. As film thickness is a linear function of the applied potential (this fact has been verified for many systems [16, 19–23, 27]):

$$L = (1-\alpha)E/\boldsymbol{E} + L_{E=0} \quad (17)$$

where α is the polarizability of the film/solution interface [21–23]; the following empirical equation [23] is mathematically equivalent to Eq. 15 and Eq. 16, respectively

$$c_O(L) = N_D(E) = w_1\exp(-bE) + w_2 \quad (18)$$

The diffusivity of oxygen vacancies is therefore calculated by the following expressions:

$$D_O = 2aJ_O/w_2\exp(zFa\boldsymbol{E}_L/RT) \quad \text{(high-field limit)} \quad (19)$$

$$D_O = RTJ_O/w_2 zF\boldsymbol{E}_L \quad \text{(low-field limit)} \quad (20)$$

The field at the metal/film interface $\boldsymbol{E}_L$ is given by the sum of all the potential drops in the system [21–23] divided by the film thickness

$$\boldsymbol{E}_L = (\phi_{M/F} + \boldsymbol{E}L + \phi_{F/S})/L \quad (21)$$

where

$$\phi_{M/F} = (1-\alpha)E - \boldsymbol{E}L$$
$$\phi_{F/S} = q_n L_{F/S}/\varepsilon\varepsilon_o \quad (22)$$

$L_{F/S}$ is the width of the metal vacancy accumulation layer and ε is the dielectric constant of the anodic film.

In analogy to Macdonald et al. [21–23], the film growth current is equal to the flux of oxygen vacancies. In the high-field limit, subject to the reasonable assumption $c_O(L) \gg c_O(0)\exp[-(L/a)]$, it is given by the expression

$$i_F \approx (2FD_O/2a)c_O(L)\exp\{(2Fa/RT)[(1-\alpha)E + q_n L_{F/S}/\varepsilon\varepsilon_0]/L\} \quad (23)$$

or, setting $A = (2FD_O/2a)c_O(L)$ and $B = (2Fa/RT)$, (24)

$$i_F = A\exp\{B[(1-\alpha)E + q_n L_{F/S}/\varepsilon\varepsilon_o]/L\} \quad (25)$$

The time dependence of the surface charge is treated in analogy to the surface charge approach [15, 16]

$$\mathrm{d}q_n/\mathrm{d}t = i_{F/S}S(q_{n,s} - q_n) \quad (26)$$

where S is a capture cross section for a positive defect by the negative surface charge.

The steady-state value of the surface charge is

$$q_{n,s} = \phi_{F/S,s}C_{F/S} = \alpha E\ \varepsilon\varepsilon_0/L_{F/S} \quad (27)$$

From (26) it follows that

$$\mathrm{d}q_n/\mathrm{d}t = i_{F/S}\ S(\alpha E\ \varepsilon\varepsilon_0/L_{F/S} - q_n) \quad (28)$$

At the steady state, the continuity equation imposes $i_F = i_{F/S} = i_s$, where i_s is the steady-state current density:

$$i_s = A\exp[B\boldsymbol{E}_s/(1-\alpha)] \quad (29)$$

From Eq. 25 and Eq. 28 under a small amplitude a.c. perturbation, assuming that the a.c. component of the current does not lead to an alteration in film thickness, we obtain:

$$\Delta i = i_s\ B[(1-\alpha)\Delta E + \Delta q_n\ L_{F/S}/\varepsilon\varepsilon_0]/L \quad (30)$$

$$\Delta q_n = i_S\ S\varepsilon\varepsilon_0\ \alpha\Delta E/\{L_{F/S}[j\omega + i_S\ S]\} \quad (31)$$

Accordingly, the faradaic impedance of the growing film is

$$\Delta i/\Delta E = i_s\ B\{(1-\alpha) + i_S\ S\varepsilon\varepsilon_0\alpha/[j\omega + i_S\ S]\}/L \quad (32)$$

which is equivalent to

$$Z_F^{-1} = 1/R_b + 1/(j\omega\ L_{sc} + R_{sc}) \quad (33)$$

where

$$R_b = L/i_s\ B(1-\alpha)$$

$$R_{sc} = L/i_s\ B\alpha$$

$$L_{sc} = L/i_s^2\ SB\alpha \quad (34)$$

To derive the total impedance, the barrier film C_b and faradaic C_0 capacitances have to be added in the appropriate manner

$$Z = [1/R_b + 1/(\ j\omega\ L_{sc} + R_{sc}) + j\omega C_b]^{-1} + 1/j\omega C_0 + R_\Omega \quad (35)$$

These capacitances are defined as

$$C_b = \varepsilon\varepsilon_o/L \quad (36)$$

$$C_0 = \lambda\Delta Q/\Delta E = (zF/V_m)\Delta L/\lambda\Delta E$$

where λ is the current efficiency for film formation [25]. The overall impedance of the system is equivalent to the electrical circuit shown in Fig. 2c.

Inserting the potential dependence of film thickness (Eq. 17) in Eqs. 34 and 36, the following relations between the physical parameters of the model and equivalent circuit elements are valid

$$i_s\ dR_b/dE = (2Fa\boldsymbol{E}_s/RT)^{-1}$$

$$dC_b^{-1}/dE = (1-\alpha)(\varepsilon\varepsilon_o E_s)^{-1}$$

$$R_b/R_{sc} = \alpha/1-\alpha$$

$$L_{sc}i_s/R_{sc} = S^{-1}$$

$$C_0 = zF(1-\alpha)/V_m\lambda E_s \quad (37)$$

Using these relations, the main parameters of film growth – steady-state field strength $\boldsymbol{E}_s$, half-jump distance a, polarizability of film/solution interface α, cross capture section S and current efficiency for film formation λ – can be determined from the potential dependence of the circuit elements.

Experimental

Electrodes and electrolytes

Spectroscopically pure Fe (Johnson Matthey, 15-ppm impurities), 99.9% Mo (Koch Laboratories) and a Fe-20 wt% Mo alloy produced from the above metals by mixing in a levitation furnace under Ar flow using a non-crucible method were used as working electrodes. The cylindrical samples were sealed in Teflon holders by acid-resistant epoxy resin in order to expose to the electrolyte a disk area of 0.072 cm^2. The electrode pretreatment consisted of mechanical polishing with emery paper grade 800, degreasing with acetone, rinsing with distilled water and cathodic polarization in the working medium. A conventional three-electrode cell featuring a platinized Pt counter electrode was used. A saturated mercurous sulphate electrode (SSE, $E_{NHE} = 0.670$ V) was employed as a reference and all the potentials in the paper are referred to it. Reagent grade 85% H_3PO_4 (Merck) served as the electrolyte and was employed in as-received condition. The measurements were accomplished at room temperature (20 ± 1°C) in naturally aerated solutions.

Apparatus and procedure

Polarization curves were traced using an M273 potentiostat driven by the M270 Electrochemical Software (Princeton Applied Research). At each potential the current – time curve was recorded until a steady state was reached. The reproducibility of the current values was ±5% . AC impedance spectra were obtained at steady state with the above potentiostat and a 5301 lock-in amplifier (Princeton Applied Research) in the high frequency region, and in the low-frequency region by a Fast Fourier Transform technique provided by the M378 Electrochemical Impedance Software (Princeton Applied Research). The frequency range was typically between 0.006 Hz and 100 KHz at an AC signal amplitude of 10 mV peak-to-peak. The reproducibility of the impedance spectra was ±2% by amplitude and ±3° by phase shift. The software for data processing and impedance simulation was elaborated by the author.

Results and discussion

Polarization curves

Figure 3 summarizes the obtained potentiostatic polarization curves of pure Fe, Mo and the Fe-20%Mo alloy in 85% H_3PO_4. The curve for Fe is qualitatively analogous to that published by Banas [26]. Four potential regions can be defined on the curves for Fe and the alloys:

1. Active dissolution domain – from the free corrosion potential to the first current plateau
2. Passivation domain – between the first and second current plateaus

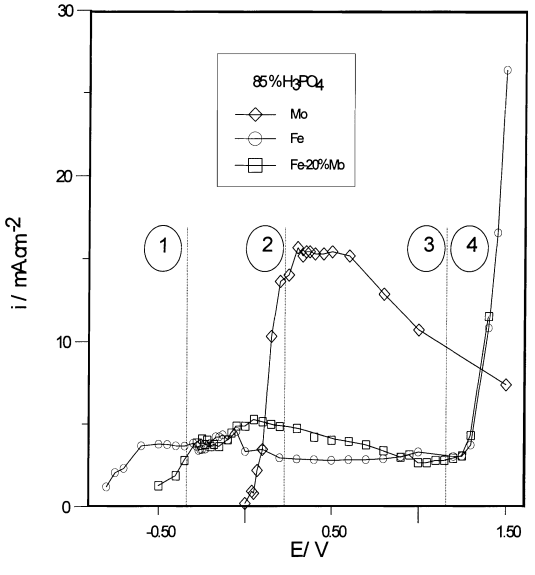

Fig. 3 Steady-state potentiostatic polarization curves of pure Fe, Mo and a Fe-20% Mo alloy in 85% H_3PO_4

3. Passivity domain coinciding with the second current plateau
4. Transpassivity domain – above the second current plateau

The polarization curve of pure Mo was commented upon in some detail in [27]. In the potential range −0.5–0.0 V molybdenum is spontaneously passive. Transpassive dissolution starts at 0.0 V and two maxima are observed at 0.4–0.5 V marking the onset of secondary passivation reactions. Then the current drops gradually to half its maximum value and a steady state is reached at ca. 2V [27]. The objective of the present paper is to model the processes in regions 2 and 3 of the polarization curves (passivation domain and passivity range).

AC impedance measurements in the passivation region

The potential dependence of the impedance spectra for pure Fe and Fe-20%Mo in 85% H_3PO_4 in the passivation region (−0.32 to 0.10 V) is presented in Fig. 4. As stated above, pure Mo is spontaneously passive in this region; therefore impedance spectra for this metal are not presented.

The spectra are somewhat analogous to those obtained for Cu in 85% H_3PO_4 [3], Fe in saturated $FeCl_2$ solutions [5, 6] and Ni, Cu, Sn and Sb in concentrated H_2SO_4 solutions [7–12]. Spectra qualitatively identical to those presented here for potentials close to −0.2 V were obtained for the passivation of pure Cr in H_2SO_4 solutions [17, 18]. The potential dependence of impedance for the Fe-20%Mo alloy is qualitatively different from that of pure iron. Circling of the origin is observed for potentials more positive than −0.20 V for the alloy, whereas for Fe this feature is detected for potentials more negative than this value. Thus different reaction paths are favoured for pure Fe and the Fe-Mo alloy in the potential range studied.

The results of the passivation model calculations are presented in the spectra of Fig. 4 with solid lines, illustrating the satisfactory agreement with experiment. The values of the kinetic parameters are summarized in Table 1 together with their standard estimation errors. The ability of the model to reproduce the potential dependences of the steady state current density, i_s, and the apparent charge transfer resistance $(R_t^{-1} + R_1^{-1})$ in the passivation domain is illustrated in Fig. 5 (for pure Fe) and Fig. 6 (Fe-20%Mo), respectively. The potential evolution of the steady state surface coverages of the intermediate species is also shown in these figures.

The accuracy in determining the kinetic constants was around 5% and statistical analysis of the non-linear least-squares fit results showed that the χ^2 criterion of model adequacy is met. The pronounced non-linearity of this system of equations and the great number of adjustable parameters do not exclude the existence of another set of kinetic constants furnishing an equally

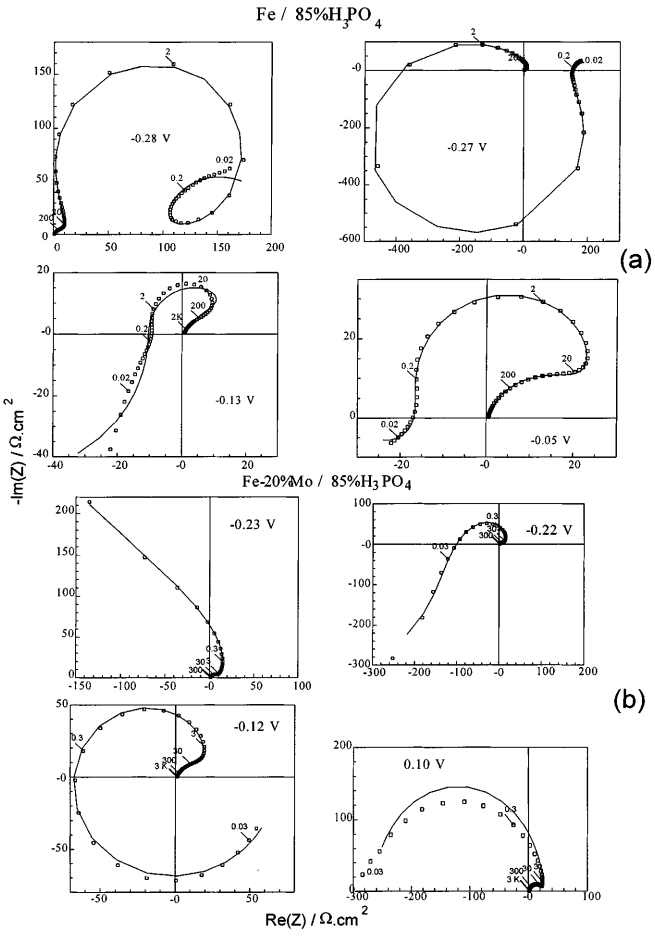

Fig. 4a, b Potential evolution of the impedance spectra in the passivation region: **a** pure Fe/85% H_3PO_4; **b** Fe-20% Mo/85% H_3PO_4. *Points* experimental values, *solid lines* best-fit calculation according to the proposed kinetic model. Parameter is frequency in hertz

good fit to the experimental results, although statistically this possibility is remote. In the case of pure Fe it was essential in order for the fitting procedure to converge that the maximum surface excess of adsorbed species was potential dependent. This was adopted in analogy to the treatment of Macdonald et al. [28] for aluminium in alkaline solution and the treatment of Bai and Conway [29] for the same metal in acetonitrile electrolyte. A possible explanation of this phenomenon is a change in the nature of the passivating species with potential or the formation of a tridimensional layer on the electrode surface. In general, the Tafel coefficients obtained are quite low (see also [28, 29]) implying a possible formation of a thin conductive film in which part of the potential drop is being consumed. The existence of such a film does not put into question the validity of the proposed model since the transfer of metal ions through it will also give rise to a pseudo-Tafel dependence of the rate constant [8].

The following conclusions can be drawn from Table 1:

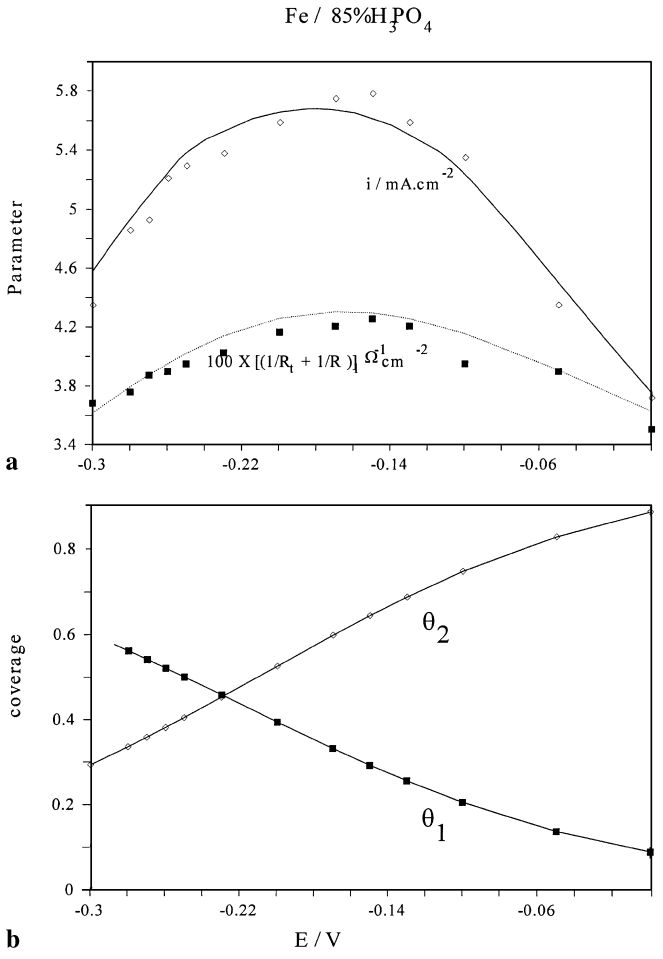

Fig. 5 a Experimental (*points*) and calculated (*solid lines*) potential dependences of the steady state current and the apparent charge transfer resistance for pure Fe/85% H_3PO_4. **b** Potential evolution of the surface coverages of the intermediate species as calculated by the proposed kinetic model

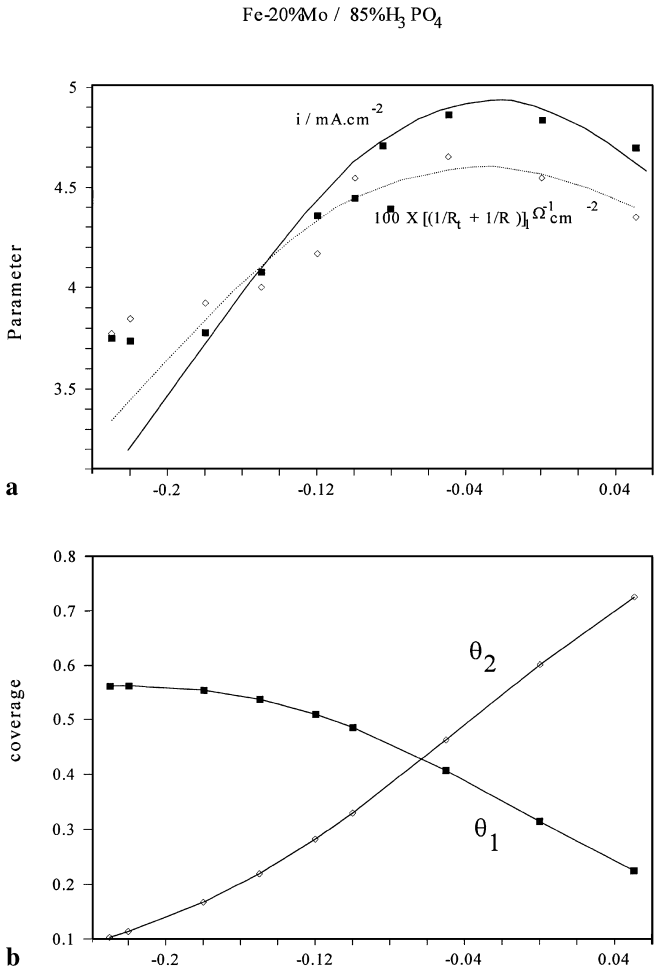

Fig. 6 a Experimental (*points*) and calculated (*solid lines*) potential dependences of the steady state current and the apparent charge transfer resistance for Fe-20% Mo/85% H_3PO_4. **b** Potential evolution of the surface coverages of the intermediate species as calculated by the proposed kinetic model

1. The standard rate constant of the second step of the active dissolution reaction increases with Mo addition, whereas the corresponding Tafel coefficient decreases. This is perhaps due to the interaction of iron and molybdenum adsorbed species.
2. Both the standard rate constant and the Tafel coefficient of the passive dissolution reaction (K_4 step) increase with Mo addition, which can be related to the occurrence of transpassive dissolution of Mo in the studied potential range affecting the stability of the passivating species $Me(II)_{pass}$.
3. Both the standard rate constant and the Tafel coefficient of the reverse reaction of step 3 increase with Mo addition, whereas the corresponding parameters of the forward reaction decrease. Thus the overall rate of the formation of passivating species is slowed down and active dissolution is favoured. This feature could also be explained by interaction between Fe and Mo adsorbed species leading to their ejection from the surface.

AC impedance measurements in the passivity range

The potential evolution of the impedance spectra of passive Fe in 85% H_3PO_4 is presented in Fig. 7a, the corresponding spectra for the passivation and secondary passivity of Mo [27] in Fig. 7b, and spectra of the passive Fe-20% Mo alloy in the same medium in Fig. 8. The high-frequency semicircle depicts the kinetics of defect migration in the bulk of the passive film, the inductive loop at medium frequencies is caused by the acceleration of this transport process by a negative surface charge at the film/solution interface, the further low-frequency capacitive loop is due to film dissolution and/or secondary film formation [16], and at the lowest frequencies the faradaic pseudocapacitance is detected. The spectra for the Fe-20% Mo alloy appear as a combination of those of the pure metals (Figs. 7 and 8). Computed impedance spectra according to the equivalent circuit (Fig. 2c) based on the kinetic model (Fig. 2a, b) are presented in Figs.7 and 8 with solid lines

Table 1 Kinetic parameters of the proposed model (Eqs. 4–9) used to simulate both the steady state polarization curves and the AC impedance diagrams for the passivation of pure Fe and Fe-20%Mo alloy in 85% H_3PO_4

Kinetic parameters	Fe 85% H_3PO_4	Standard error (%)	Fe-20%Mo/ 85% H_3PO_4	Standard error (%)
K_1^0 mol $\cdot$ cm^{-2}s^{-1}	5×10^{-8}	3.4	1×10^{-8}	4.5
K_2^0 mol $\cdot$ cm^{-2}s^{-1}	6×10^{-9}	2.3	1.5×10^{-8}	2.5
K_3^0 mol $\cdot$ cm^{-2}s^{-1}	3.3×10^{-8}	5.5	2.5×10^{-8}	3.1
K_{-3}^0 mol $\cdot$ cm^{-2}s^{-1}	1.5×10^{-6}	3.1	4.5×10^{-6}	5.5
K_4^0 mol $\cdot$ cm^{-2}s^{-1}	2×10^{-9}	6.5	3×10^{-9}	7.2
b_1 V^{-1}	4	2.2	6	1.5
b_2 V^{-1}	5.3	3.5	2.6	3.1
b_3 V^{-1}	5.6	2.2	6	2.5
b_{-3} V^{-1}	4.2	4.1	5.2	4.0
b_4 V^{-1}	2	5.0	3	5.0
β mol $\cdot$ cm^{-2}(−0.3 V)	1×10^{-8}	fixed	4×10^{-8}	fixed
β mol $\cdot$ cm^{-2}(0.0 V)	4×10^{-8}	fixed	4×10^{-8}	fixed

illustrating the satisfactory agreement with the experiment. The potential dependences of the main circuit elements are collected in Fig. 9 (pure Mo/85% H_3PO_4) and Fig. 10 (pure Fe and Fe-20% Mo/85% H_3PO_4), respectively.

For pure Mo, there is full agreement between the predictions of Eqs. 37 of the Theory section and the experimental potential dependences of the circuit elements (Fig. 9) (the value of the faradaic pseudocapacitance was found to be constant in the potential range 2–10 V and equal to 6.6 mF $\cdot$ cm^{-2} [27]). The low frequency capacitive time constant is not observed for the secondary passive state of this metal; thus probably no secondary outer layer formation takes place in the system [16, 27]. This suggestion is supported by the

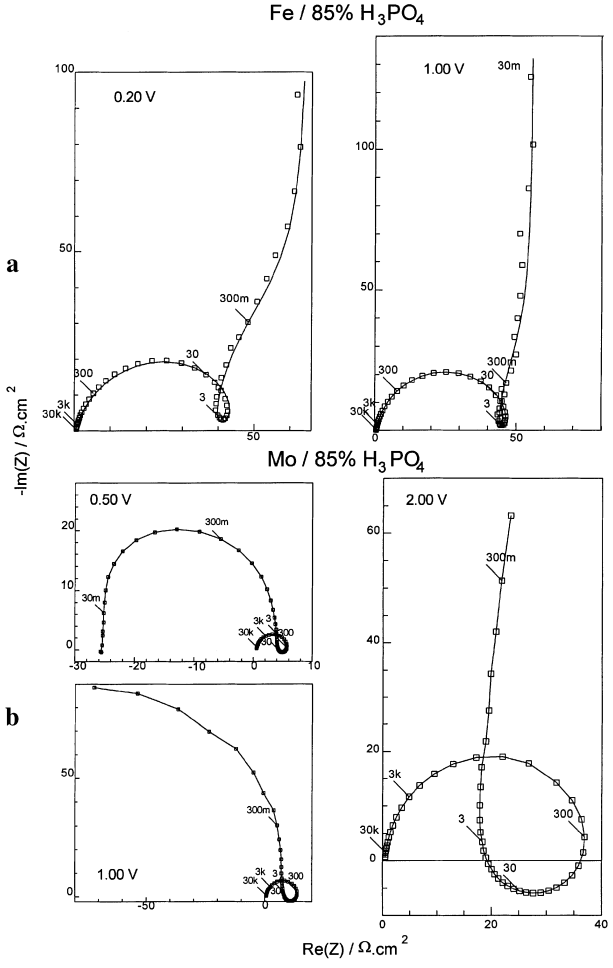

Fig. 7a,b Potential evolution of the impedance spectra in the passivity range: **a** pure Fe/85% H_3PO_4, **b** pure Mo/85% H_3PO_4. *Points* experimental values, *solid lines* best-fit calculation according to the proposed kinetic model. Parameter is frequency in hertz

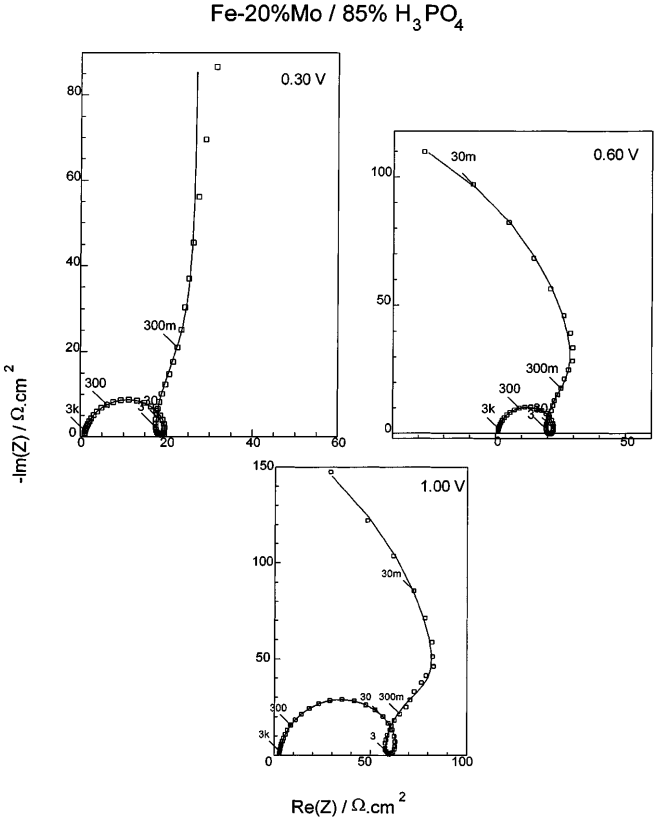

Fig. 8 Potential evolution of the impedance spectra in the passivity range: Fe-20% Mo/85% H_3PO_4. *Points* experimental values, *solid lines* best-fit calculation according to the proposed kinetic model. Parameter is frequency in hertz

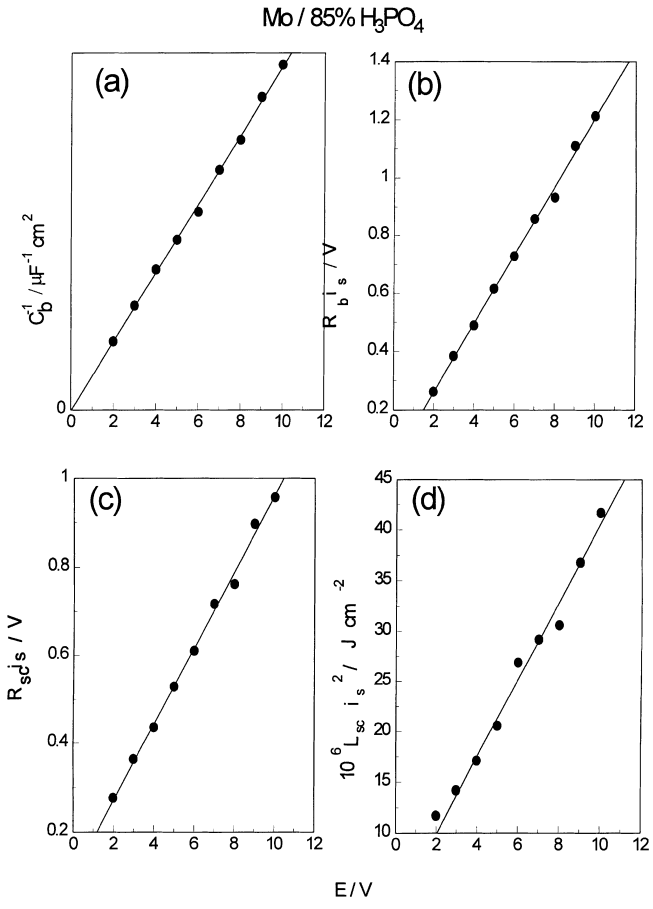

Fig. 9a-d Potential dependences of the parameters of the equivalent electrical circuit proposed within the frames of the surface charge approach (Fig. 2c) for pure Mo/85% H_3PO_4

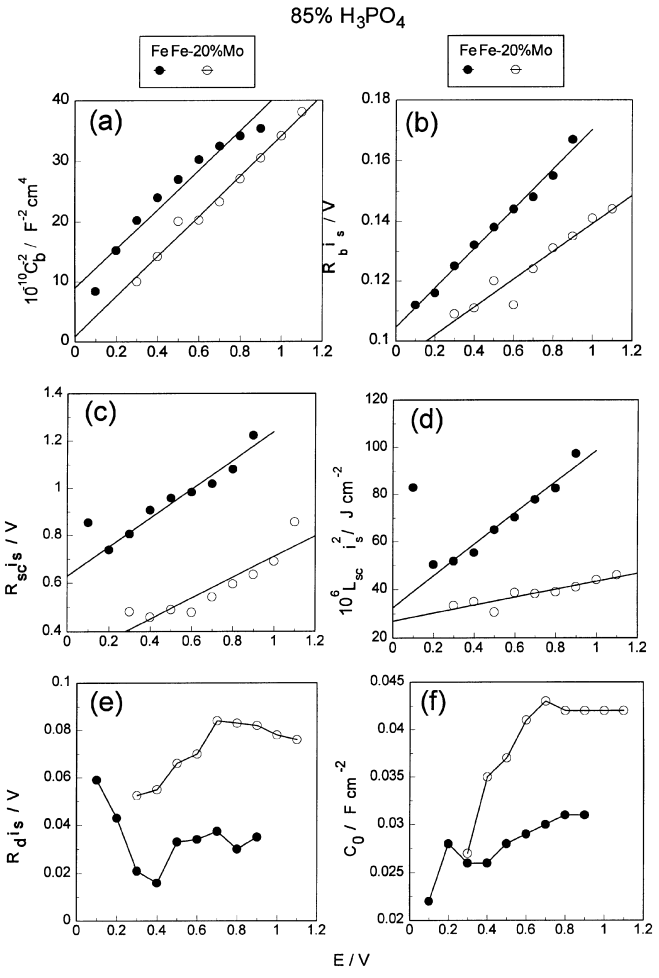

Fig. 10a-f Potential dependences of the parameters of the equivalent electrical circuit proposed within the frames of the surface charge approach (Fig. 2c) for pure Fe and the Fe-20% Mo alloy in 85% H_3PO_4

potential independence of the faradaic pseudocapacitance C_0. Assuming reasonable values for the molar volume of the phase in the anodic layer and its dielectric permittivity ($\varepsilon = 29.4$ and $V_m = 31.1 cm^3 \cdot mol^{-1}$ [27]), the main kinetic and structural parameters of the Mo/anodic layer/electrolyte system are determined. These parameters are collected in Table 2 together with the estimation accuracy. They are analogous to those computed for a range of passive metals [13–16, 33]. The polarizability of the film/solution interface is close to 0.5, as found for several metal/passive film/solution systems within the frames of the Point Defect Model [19, 23]. The value of the field strength confirms the validity of the high-field limit.

For pure Fe and the Fe-20% Mo alloy, conversely, the reciprocal capacitance of the film does not obey a linear but a square dependence on the electrode potential, suggesting a Mott-Schottky behaviour (Fig. 10a). Thus the major part of the potential drop is probably located in the n-semiconductor region adjacent to the metal/film interface (Fig. 2a,b). This fact is supported by

Table 2 Kinetic parameters of the proposed model (Eqs. 32–37) used to stimulate the a.c. impedance diagrams for the passive state of pure Fe, Mo and Fe-20%Mo alloy in 85% H_3PO_4

Model parameters	Mo 85% H_3PO_4	Standard error (%)	Fe 85% H_3PO_4	Standard error (%)	Fe-20%Mo/ 85% H_3PO_4	Standard error (%)
E_L/MV · cm^{-1}	1.1	1.5	3.0	2.0	3.6	2.5
a nm	0.30	4.5	0.50	fixed	0.50	fixed
α	0.58	3.5	0.10	2.5	0.10	3.7
S $mC^{-1} \cdot cm^2$	22.3	1.5	9.2	2.2	26.4	1.8
ε	29.4	fixed	15.6	fixed	15.6	fixed

the low value of the polarizability of the film/solution interface (Table 2) as computed from the potential dependence of the equivalent circuit elements (Fig. 2c and Eq. 37). Assuming a dielectric constant of the anodic layer of 15.6 [30], it is possible to estimate the donor density at the interface $\left(3 \cdot 10^{20}\mathrm{cm}^{-3}\right)$ from the Mott-Schottky slopes in Fig. 10a (these slopes are identical for Fe and the alloy within experimental error). This value is close to that estimated by Schmuki et al.[31] using reduction doping of bulk Fe_2O_3 electrodes and comparing them to the passive layer on Fe in borate buffer. The linearity of the Mott-Schottky plots implies that the value of the donor density is independent of potential in the passive range. To estimate the value of the diffusivity of vacancies, Eq. 19 is rewritten in the approximate form

$$D_{\mathrm{O}} \approx 2aJ_{\mathrm{O}}/N_{\mathrm{D}} \exp(zFa\boldsymbol{E}_{\mathrm{L}}/RT)$$

The obtained value of $(2 \pm 1) \cdot 10^{-17}\mathrm{cm}^2\ \mathrm{s}^{-1}$ is ca. two orders of magnitude higher than that estimated by Macdonald and Smedley [32] for the cation vacancy diffusivity in the passive film on Ni in phosphate solutions. It is worth noting that a value of similar magnitude was obtained for the anodic layer on W in 1M H_3PO_4 by the present author [33]. This seems to be a proof of the parent nature of the current-carrying species in anodic films on W, Fe and the Fe-Mo alloy.

The slope of the potential dependence of the product $R_{\mathrm{b}}i_{\mathrm{s}}$ for pure Fe coincides with that obtained for the same metal in a range of acidic phosphate and sulphate solutions [34], being about 30% smaller for the Fe-20% Mo alloy (Fig. 10b). Assuming a value of the half-jump distance $a = 0.5$ nm [34], the field strength for Fe and the alloy is estimated and the values are collected in Table 2. They confirm once again the validity of the high-field limit of the vacancy migration mechanism. The value of the capture cross section for an oxygen vacancy by the negative surface charge S is ca. three times as high for the anodic film formed on the alloy electrode as that for the film formed on pure Fe. This points to a more disordered structure for the layer grown on the Fe-20% Mo substrate.

In contrast to pure Mo, a low frequency capacitive time constant is observed both for Fe and the Fe-20% Mo alloy, and the potential evolution of the product of its resistance R_{d} and the steady-state current is presented in Fig. 10e. The corresponding dependence of the faradaic pseudocapacitance C_0 is shown in Fig. 10f. For pure Fe, the product $R_{\mathrm{d}}i_{\mathrm{s}}$ decreases with potential and a steady state is reached at 0.4–0.5 V (Fig. 10e). The faradaic pseudocapacitance increases slightly to a stationary value at 0.7–0.9 V (Fig. 10f), i.e. the efficiency of film formation reaches a constant value. For the Fe-20% Mo alloy, both product $R_{\mathrm{d}}i_{\mathrm{s}}$ and C_0 increase with potential, their values being 2–3 times as high as those for pure Fe. This difference can be related to the existence of another process taking place on the alloy electrode in the potential range 0.5–1.1 V and characterized by the lowest frequency loop exhibiting a negative resistance (Fig. 8). This process probably represents some kind of transformation of the anodic layer (e.g. dehydration, alteration of the cation valency state) which leads to the increase of its specific resistivity and hence the decrease of the steady-state current with increase of potential (Fig. 3) which is tantamount to a negative resistance.

Conclusions

Two models describing the successive stages of the establishment and stabilization of the passive state in concentrated acid solutions via the formation and subsequent growth of anodic oxide films on metals and alloys are presented. The first one assumes the parallel occurrence of dissolution and passivation reactions on the metal surface by competitive adsorption of water and acid anions on active substrate sites. It is able to reproduce quantitatively the complicated type of impedance locus widely observed on metals in concentrated solutions, i.e. circling of the low-frequency data of the spectrum around the origin of the complex plane. Based on the assumptions of Langmuir type adsorption and Tafel-like potential dependence of the rate constants a procedure for the determination of the model parameters by using a combination of the equivalent circuit and physical model approaches is proposed. The second model is an update of the so-called surface charge approach to build up a bridge between its line of reasoning and the most elaborated quantitative model of the passive state – the point defect model (PDM) of D.D. Macdonald and co-workers. The updated approach is based on the chemistry of the PDM and accepts that the field strength is independent of potential and thickness (proposed within its framework) as well as the assumption that most anodic oxides grow mainly via migration of oxygen vacancies. The transport of point defects, however, is treated using general motion equations under the influence of electric field of any magnitude and especially the high-field approximation. The migration of oxygen vacancies is assumed to be enhanced by a negative surface charge formed by accumulation of metal vacancies generated at the film/solution interface. Possible reactions of film dissolution and secondary layer formation are taken into account as well. In its present form, the proposed model gives the possibility of estimating the main kinetic and structural characteristics of the metal/anodic oxide film/electrolyte system in the passive state for a range of metals and alloys.

References

1. Landolt D (1987) Electrochim Acta 32: 1
2. Epelboin I (1966) In: Proceedings of surface 66. Foster. Zurich, p 161
3. Glarum SH, Marshall JH (1985) J Electrochem Soc 132: 2878

4. Clerc C, Landolt D (1988) Electrochim Acta 33: 859
5. Grimm RD, West AC, Landolt D (1992) J Electrochem Soc 139: 1622
6. West AC, Grimm RD, Landolt D, Deslouis C, Tribollet B (1992) J Electroanal Chem 330: 693
7. Epelboin I, Keddam M (1972) Electrochim Acta 17: 177
8. Keddam M, Takenouti H, Yu N (1985) J Electrochem Soc 132: 2561
9. Bojinov M (1994) PhD thesis, Bulgarian Academy of Sciences, Sofia
10. Bojinov M, Salmi K, Sundholm G (1993) J Electroanal Chem 347: 207
11. Bojinov M, Salmi K, Sundholm G (1993) J Electroanal Chem 358: 177
12. Bojinov M (1996) J Electroanal Chem 405: 15
13. Bojinov M, Kanazirski I, Girginov A (1992) Electrochim Acta 37: 2415
14. Kanazirski I, Bojinov M, Girginov A (1993) Electrochim Acta 38: 1061
15. Bojinov M (1995) Materials Sci Forum 185–188: 601
16. Bojinov M, Kanazirski I, Girginov A (1996) Electrochim Acta 41: 2695
17. Dobbelaar JAL, De Wit JHW (1990) J Electrochem Soc 137: 2038
18. Dobbelaar JAL De, Wit JHW (1992) J Electrochem Soc 139: 716
19. Macdonald DD, Biaggio SR, Song H (1992) J Electrochem Soc 139: 170
20. Goossens A, Macdonald DD (1993) J Electroanal Chem 352: 68
21. Macdonald DD, Sikora E, Sikora J (1994) In: Hebert KR, Thompson GE (eds) Proceedings of 7th International Symposium on Oxide films on metals and alloys. The Electrochemical Society, Princeton, NJ, p 139
22. Sikora J, Sikora E, Macdonald DD (1994) In: Hebert KR, Thompson GE (eds) Proceedings of 7th International Symposium on Oxide films on metals and alloys. The Electrochemical Society, Princeton, NJ, p 268
23. Sikora E, Sikora J, Macdonald DD (1996) Electrochim Acta 41: 783
24. Fromhold AT Jr (1976) In: Diggle JW, Vijh AK (eds) Oxides and oxide films, vol 3. Dekker, New York, pp 1–271
25. De Wit HJ, Wijenberg C, Crevecoeur C (1979) J Electrochem Soc 126: 779
26. Banas J (1995) Materials Sci Forum 185–188: 845
27. Bojinov M, Betova I, Raicheff R (1996) J Electroanal Chem 411: 37
28. Macdonald DD, Real S, Smedley SI, Urquidi-Macdonald M (1988) J Electrochem Soc 135: 2410
29. Bai L, Conway B (1990) J Electrochem Soc 137: 3737
30. Simoes AMP, Ferreira MGS, Rondot B, Da Cunha Belo M (1992) Materials Sci Forum 111–112: 303
31. Schmuki P, Buechler M, Virtanen S, Boehni H, Mueller R, Gauckler LJ (1995) J Electrochem Soc 142: 3336
32. Macdonald DD, Smedley SI (1990) Electrochim Acta 35: 1949
33. Bojinov M (1997) Electrochim Acta (accepted for publication)
34. Keddam M, Lizee J-F, Pallotta C, Takenouti H (1984) J Electrochem Soc 131: 2016